

Nanoscale fracture of tetrahedral amorphous carbon by molecular dynamics: Flaw size insensitivity

Qiang Lu,¹ Nigel Marks,² George C. Schatz,³ and Ted Belytschko^{1,*}

¹*Department of Mechanical Engineering, Northwestern University, 2145 Sheridan Road, Evanston, Illinois 60208-3111, USA*

²*School of Physics A28, The University of Sydney, New South Wales 2006, Australia*

³*Department of Chemistry, Northwestern University, 2145 Sheridan Road, Evanston, Illinois 60208-3113, USA*

(Received 18 May 2007; published 25 January 2008)

The fracture of tetrahedral amorphous carbon at the nanoscale was investigated with molecular dynamics simulations using the environment-dependent interatomic potential. It was found that the fracture strength of amorphous carbon nanospecimens is insensitive to initial cracks with diameters smaller than about 40 Å, i.e., the material exhibits flaw tolerance at the nanoscale. It was also found that amorphous carbon nanospecimens fracture very differently from diamond; (i) failure is gradual instead of catastrophic and (ii) it is accompanied with voidlike defect growth and coalescence. This fracture behavior appears to result from the structural disorder of amorphous carbon. In order to further explore the effect of crack size in materials with structural disorder, larger two-dimensional random network models were studied and found to also exhibit void growth during fracture and flaw tolerance.

DOI: [10.1103/PhysRevB.77.014109](https://doi.org/10.1103/PhysRevB.77.014109)

PACS number(s): 61.43.Er, 81.05.Uw, 62.20.M-

I. BACKGROUND

Tetrahedral amorphous carbon (ta-C) is a form of amorphous carbon containing a significant fraction of sp^3 bonds. It has drawn considerable interest because of its desirable mechanical, thermal, and electronic properties, many of which are comparable to those of diamond.¹

In this paper, we report molecular dynamics simulations of the fracture of ta-C nanospecimens (hereafter, we refer to them as simply amorphous carbon). We found that amorphous carbon nanospecimens are weaker than diamond and that their fracture is more gradual and accompanied by nucleation and coalescence of voidlike defects. Most interesting is that, in contrast to diamond, amorphous carbon nanospecimens appear to exhibit flaw tolerance: cracklike defects smaller than 40 Å have almost no effect on the fracture strength. Flaw tolerance at the nanoscale was previously predicted by Gao *et al.* for biological crystalline materials such as bone, tooth, and nacre.²

These differences between fracture in amorphous carbon and diamond appear to be due to the structural disorder of the former. To further elucidate this hypothesis and examine flaw tolerance for larger specimens, we studied larger two-dimensional random networks with a simpler potential. We found analogous behavior in these networks: more gradual failure, void formation, and flaw tolerance. It appears that flaw tolerance may be a characteristic of disordered atomic structures at the nanoscale.

Before proceeding, we briefly review the relevant literature. Fyta *et al.*,³ using tight-binding quantum methods, computed fracture strengths of 50–90 GPa and fracture strains of 0.10–0.12 for amorphous carbon. Paci *et al.*,⁴ using several quantum mechanics (QM) methods, calculated fracture strength of a diamond cluster containing an amorphous carbon region and reported fracture strength of 61–86 GPa and fracture strains of 0.13–0.16. Both theoretical results differ substantially from experimental fracture strengths of 6–9 GPa and fracture strains of 1.2%.¹ Such differences may

be due to defects in the experimental specimens. For example, even in nanotubes, differences between experimental and theoretical strengths are greater than 50% due to vacancies, holes, and slitlike defects.^{5–10} For ultrananocrystalline diamond (UNCD), in which an amorphouslike phase occurs between grains and failure is usually intergranular, Espinosa *et al.*¹¹ reported experimental fracture strengths between 0.89 and 2.26 GPa. Paci *et al.*,¹² using density functional theory (DFT), computed the intergranular strength of diamond to be 100 GPa. The role of flaws on fracture strength has also been studied for diamond,¹³ UNCD,¹² and amorphous metals.¹⁴

In our molecular dynamics simulations of the fracture of amorphous, we used the environment-dependent interatomic potential¹⁵ (EDIP) which was specifically developed for amorphous carbon. We show that the widely used Tersoff potential¹⁶ and the Brenner potentials^{17,18} fail to provide the correct sp^3 fractions in the synthesis of amorphous carbon; this was also noted in deposition simulations.¹⁹ EDIP has been successfully used in other applications, such as liquid quenching and thin film deposition.^{20–22}

This paper is organized as follows. In Sec. II, the effectiveness of the EDIP and Brenner and Tersoff potentials for amorphous are compared; in Sec. III, we examine the fracture of pristine and defective amorphous carbon, and diamond; in Sec. IV, we show the similarities of the fracture of two-dimensional random networks to that of amorphous carbon and study larger defects in the former; conclusions are drawn in Sec. V.

II. STUDY OF ENVIRONMENT-DEPENDENT INTERATOMIC POTENTIAL PERFORMANCE FOR AMORPHOUS CARBON

As a preliminary step, we examined the ability of several commonly used potentials for carbon, EDIP,¹⁵ the Tersoff potential,¹⁶ and the Brenner second-generation reactive empirical bond order (REBO) potential,¹⁷ to model amorphous carbon. We examined the performance of these potentials in

TABLE I. Mechanical properties obtained by the Brenner REBO (Ref. 17) and Tersoff (Ref. 16) potentials and EDIP (Ref. 15) compared with tight-binding (Ref. 5) and quantum mechanics methods (Ref. 4) and experiments (Ref. 1) E is Young's modulus, σ_{\max} is the fracture stress, and ε_f is the fracture strain.

	Brenner REBO potential	Tersoff potential	EDIP	Tight-binding methods		Quantum mechanics methods	Experiment
sp^3 (%)	27	30	60	50	80	50	N/A
Number of atoms	2016	2016	2016	512	512	119	N/A
E (GPa)	~300	~300	~700	~500	~1000	690–780	600–900
σ_{\max} (GPa)	40	36	52.2	30	45	61–86	6–9
ε_f	0.45	0.48	0.12	0.11	0.12	0.13–0.16	0.01

the numerical synthesis of amorphous carbon by simulated annealing. A crystalline diamond specimen was heated above its melting point (3820 K) and then slowly cooled to room temperature at a rate of 200 K/ps to obtain amorphous carbon. The specimen was a parallelepiped of 2016 atoms with initial dimensions of $17.62 \times 17.60 \times 36.96 \text{ \AA}^3$; after cooling, its dimensions were $18.62 \times 18.81 \times 39.50 \text{ \AA}^3$ and its density was 2.90 g/cm^3 . Periodic boundary conditions were applied in all directions during the process. Three specimens were considered and the mean is reported.

The bonding fraction is compared for various potentials and with tight binding³ in Table I. The sp^3 fraction was taken to be the fraction of fourfold coordinated atoms, though in EDIP, the coordination is calculated with a functional which can describe distorted configurations involving π electrons. We found that the Tersoff and REBO potentials failed to generate reasonable amorphous structures. As shown in Table I, the sp^3 fractions generated with these two potentials were less than 30%, which is much smaller than experimental data, which are usually greater than 75%. The EDIP method gives significantly better results (sp^3 fractions of 50%–60%), though these are still lower than the experimental data. EDIP provides better transferability because its functional form is parametrized by *ab initio* data for the graphite/diamond transformation, thus providing an accurate description of the energetics of bond making and breaking. EDIP also includes nonbonded π -electron interactions which control the density of graphite. The absence of these interactions in the Tersoff and Brenner simulations may result in structures with unphysically high sp^2 fractions at this density.

Next, we obtained the elastic modulus, failure strain, and failure strength for the above specimen ($18.62 \times 18.81 \times 39.50 \text{ \AA}^3$) for the three potentials. In these and all subsequent data in this paper, an engineering definition of stress and strain is used, so the stress σ is given by $\sigma = P/A$, where P is the total force acting on the specimen, and A is the cross-sectional area of the specimen prior to application of the load. The force P was computed by summing the z components of the bond forces on atoms with prescribed displacements. The strain is defined by $\varepsilon = (L_z - L_z^0)/L_z^0$, where L_z and L_z^0 are the current and initial lengths in the z direction of the specimen, respectively. Young's modulus was obtained from the initial slope of the stress-strain curve.

As can be seen from Table I, the stiffness and fracture strength obtained with the Tersoff and REBO potentials are much lower than those obtained by tight-binding methods³ and quantum mechanics methods,⁴ whereas EDIP agrees better.

To examine the performance of EDIP for other carbon-based nanostructures, we also studied diamond nanospecimens and nanotubes with these three potentials. For nanotubes, a crystalline form of carbon, the Brenner potential has been shown to agree reasonably well with DFT and PM3 quantum mechanics calculations,^{8,9} although it does tend to underestimate both stiffness and strength. In the simulations reported in Table II, the diamond specimen (2016 atoms, $18.62 \times 18.81 \times 39.50 \text{ \AA}^3$) was loaded in the $\langle 111 \rangle$ direction. The molecular dynamics (MD) simulations were conducted at 1 K and the displacements were prescribed at a rate of 0.014/ps; molecular mechanics (MM) simulations (equilibrium solutions obtained by energy minimization) were also made. Although there are some differences between the results, the MD results with EDIP are clearly acceptable.

III. FRACTURE OF TETRAHEDRAL AMORPHOUS CARBON

A. Pristine amorphous carbon specimens

In the following, we describe MD simulations of pristine and defected amorphous carbon specimens. The results were obtained by molecular dynamics simulations because it was

TABLE II. Material and fracture properties of a pristine diamond cluster, with 2016 atoms, $17.42 \times 17.60 \times 36.96 \text{ \AA}^3$ in dimension, and fracture plane (111), obtained by MM and MD with the REBO potential and EDIP. E is Young's modulus, σ_{\max} is the fracture stress, and ε_f is the fracture strain.

	Molecular mechanics		Molecular dynamics	
	REBO potential	EDIP	REBO potential	EDIP
E (GPa)	1250	1040	1200	1020
σ_{\max} (GPa)	95.5	84.8	95.0	86.5
ε_f	0.13	0.16	0.13	0.16

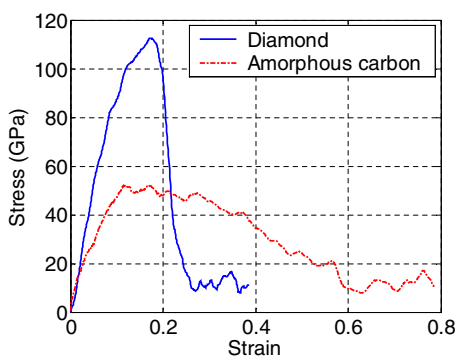


FIG. 1. (Color online) Stress-strain curves for tensile loading simulations of an amorphous carbon cluster and a diamond cluster at 0.014/ps. The data were filtered by a 20-point average filter.

very difficult to obtain convergence with molecular mechanics (i.e., zero temperature methods). The specimen was of the same size as in the previous section. The specimens were loaded at a constant strain rate (0.014/ps) until failure at 300 K with a linear-scaling temperature control. We tested several strain rates and found that the fracture properties do not change significantly for smaller loading rates. The loading was applied by prescribing the displacement of the atoms on the two opposing ends (along the longest dimension) of the specimen at a constant speed. The prescribed displacements were imposed over a thickness of 3.70 Å, i.e., over about two layers of atoms. The lateral boundaries were free for the intent here was to model nanospecimens. Stress-strain curves that are shown were filtered by a 20-point average filter. The cut-off distance for the EDIP force calculation was 1.84 Å; this distance was also the criterion for bond breaking.

The stress-strain curve for the amorphous carbon nanospecimen is shown in Fig. 1. The maximum stress (52.2 GPa) is defined as the fracture stress. The corresponding strain (12%) is defined as the fracture strain. Young’s modulus is obtained from the initial slope of the filtered stress-strain curve, which is around 700 GPa; this agrees well with the tight-binding results by Fyta *et al.* (see Table I).

The stress-strain curve has four clear stages: (a) the stress increases approximately linearly to about 12% strain; (b) the slope of the stress-strain curve suddenly becomes negative, and the stress decreases gradually by about 10%, while the strain increases from 12% to about 27%; (c) the stress decreases more rapidly for strains between 27% and 60%; (d) the stress is approximately constant at 10 GPa as the strain increases from 60% to 80%. The behavior in stages (b) and (c) is often called strain softening in the engineering literature; it is characteristic of an unstable material.

Figures 2(a)–2(c) show stick models and Figs. 2(A)–(C) show the fourfold coordinated carbon atoms, respectively, in the specimen at various stages of the loading: (i) the initial state, (ii) at maximum stress (12% strain), (iii) after the initial gradual softening stage (27% strain), and (iv) at maximum (79%) strain. The depiction of atoms with coordination of 4 clarifies defect development since all atoms connected to fewer than three neighboring atoms are not shown.

As can be seen, at zero strain, there are several local regions with short-range order and there are no large defects.

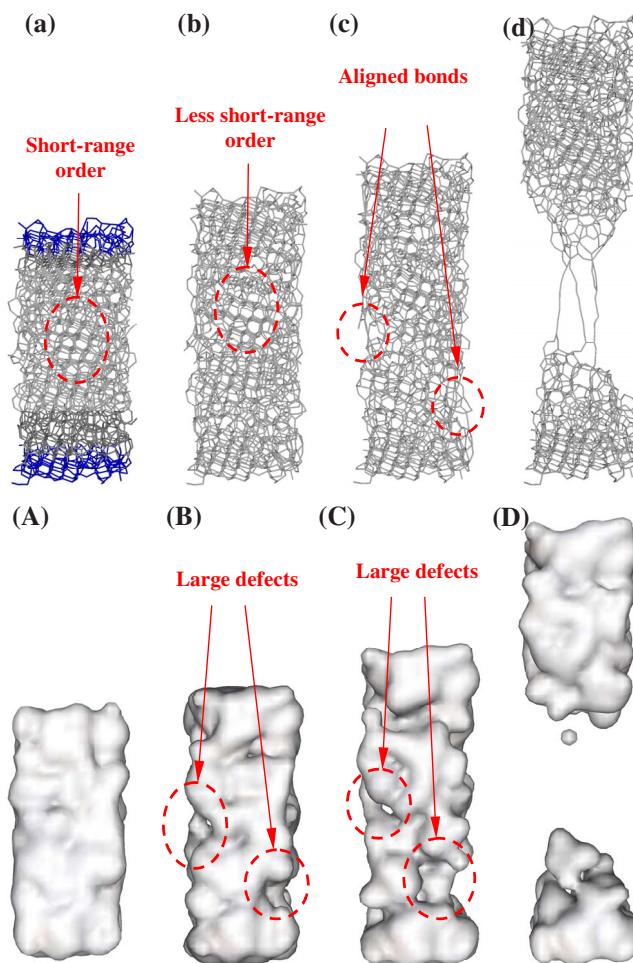


FIG. 2. (Color online) [(a)–(d)] Stick models and [(A)–(D)] surfaces of fourfold coordinated atoms of the amorphous nanospecimen during the fracture process: [(a) and (A)] at 0 strain (with boundary atoms in dark blue), [(b) and (B)] at maximum stress, 12% strain, [(c) and (C)] at 27% strain, and [(d) and (D)] at 79% strain.

At the maximum stress [Fig. 2(b)], the domains with short-range order have shrunk, and defects have nucleated inside the specimen. Two larger voidlike defects have formed on each side, as shown in coordinated atom depiction [Fig. 2(B)]. These are not true voids but regions of lower bond densities, and hence lower strength. Subsequently, short-range order totally disappears, and some atomic bonds are rotated to align with the loading direction, as shown in Fig. 2(c). At the same time, the defects grow significantly [Fig. 2(C)]. In Fig. 2(d), the two parts of the specimen are almost completely separated except for three carbon-carbon chains. It can be seen from Fig. 1 that these chains sustain about 10 GPa of stress.

Similar carbon single bond chain formation has been observed in several experiments²³ and theoretical studies of the fracture of amorphous carbon structures⁴ and carbon nanotubes.^{23,24} The tendency toward structural rearrangement substantially toughens the amorphous carbon. While the stages after the maximum stress have no influence on the strength, they increase the energy dissipation associated with the failure, and hence the toughness.

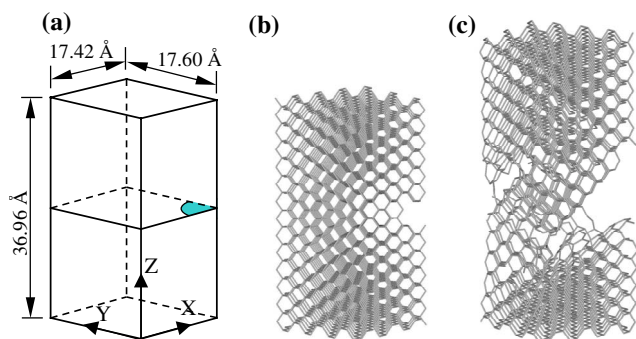


FIG. 3. (Color online) (a) Crack (twofold symmetry of the y - z plane is used), (b) structure at 0 strain, and (c) right after maximum force point.

We next compare the fracture process in amorphous carbon with that of diamond. Here, we consider fracture in a $\langle 110 \rangle$ plane for a similar nanospecimen: the number of atoms, temperature control, molecular potential, and loading speed are identical to those used for amorphous carbon. The stress-strain curve is shown in Fig. 1 together with that of the amorphous carbon nanospecimen. The diamond fractures in a catastrophic manner: the stress increases monotonically to a peak (at a strain of 17.4%) and then drops suddenly to about 10 GPa. This sudden drop in the stress corresponds to a rapid growth of the crack from a few broken bonds to almost complete separation of the body.

Such catastrophic failure has also been observed in simulations of carbon nanotubes and graphene by MM.⁸ In fact, in QM simulations,^{8,9} equilibrium configurations were not found after the fracture stress.

B. Effects of initial cracks on amorphous carbon fracture

We next examine the effect of cracklike defects on the strength of amorphous carbon and diamond. The amorphous carbon and diamond samples are identical to those in the previous subsection, except that penny-shaped cracks of radii of 6.0–45 Å are inserted. The cracks were created by removing a penny-shaped section of carbon atoms at one edge of the cylinder; such cracks are usually called edge cracks, as shown in Fig. 3. Note that we did not simply break the bonds cut by the plane of crack because this is unrealistic for modeling of initial cracks (see Ref. 8).

The diamond nanospecimen with a circular edge crack is shown in Fig. 3(a). The atomic structures of the specimen at zero strain and immediately after the fracture are shown in Figs. 3(b) and 3(c), respectively. The stress-strain curves for both pristine diamond and the diamond specimen with an initial crack are shown in Fig. 4. The fracture stress and strain are easily identified from the peaks and sudden drops in the stress-strain curves. The crack decreases the fracture strength from 112.8 to 91.3 GPa (a 19% decrease) and the ultimate strain from 17.4% to 14.7%. From Figs. 3(b) and 3(c), we see that immediately after the maximum stress, a plane of bonds in the (111) plane are broken, i.e., the crack has quickly grown across almost the entire specimen.

In contrast, the stress-strain curves for pristine amorphous carbon and precracked amorphous carbon, shown in Fig. 5,

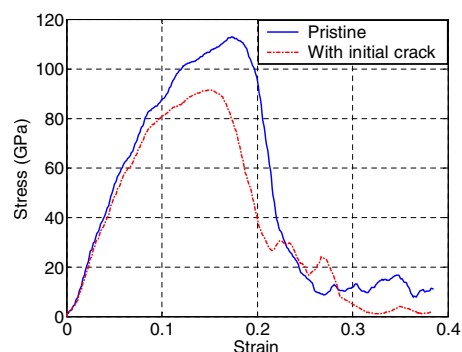


FIG. 4. (Color online) Stress-strain curve for pristine diamond and diamond with an initial crack of radius of 6 Å.

hardly differ until the maximum stress is reached. The fracture strength only decreases from 52.2 to 51.4 GPa, and the fracture strain is also almost unchanged.

The fracture process of the amorphous carbon with an initial crack of radius of 6 Å is illustrated in Fig. 6. Comparing the fracture processes of amorphous carbon clusters with and without the initial crack (Figs. 6 and 2), it can be seen that similar large voidlike defects develop. Apparently, the initial crack does not alter the evolution of the atomic structure significantly until after the maximum stress is reached. This may explain why the effect of the initial crack on the fracture stress and strain is insignificant. However, after the maximum stress, the evolution of the atomic structure [Figs. 6(c) and (C) and 6(d) and (D)] differs from that of the pristine specimen (Fig. 2).

The differences between fracture of amorphous carbon and diamond are as follows:

- (i) While the fracture of diamond is catastrophic, characterized by a sudden drop of stress, the stress in amorphous carbon decreases gradually after the fracture stress.
- (ii) The fracture strength of amorphous carbon is significantly lower than that of diamond.
- (iii) The fracture strain of amorphous carbon is smaller than that of diamond. However, the strain at which the amorphous carbon specimen is completely broken is much larger than that of diamond.
- (iv) Various defects, such as cracks and voidlike defects with lower bond densities, develop during the failure process of amorphous carbon. The growth and coalescence of these

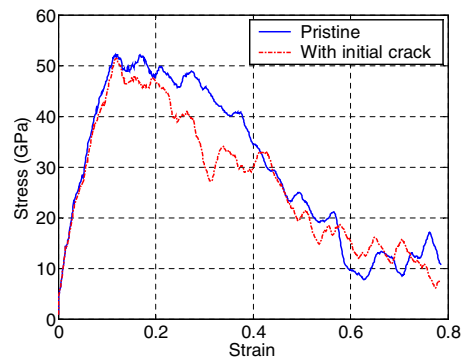


FIG. 5. (Color online) Stress-strain curve for pristine amorphous carbon and amorphous carbon with an initial crack of radius of 6 Å.

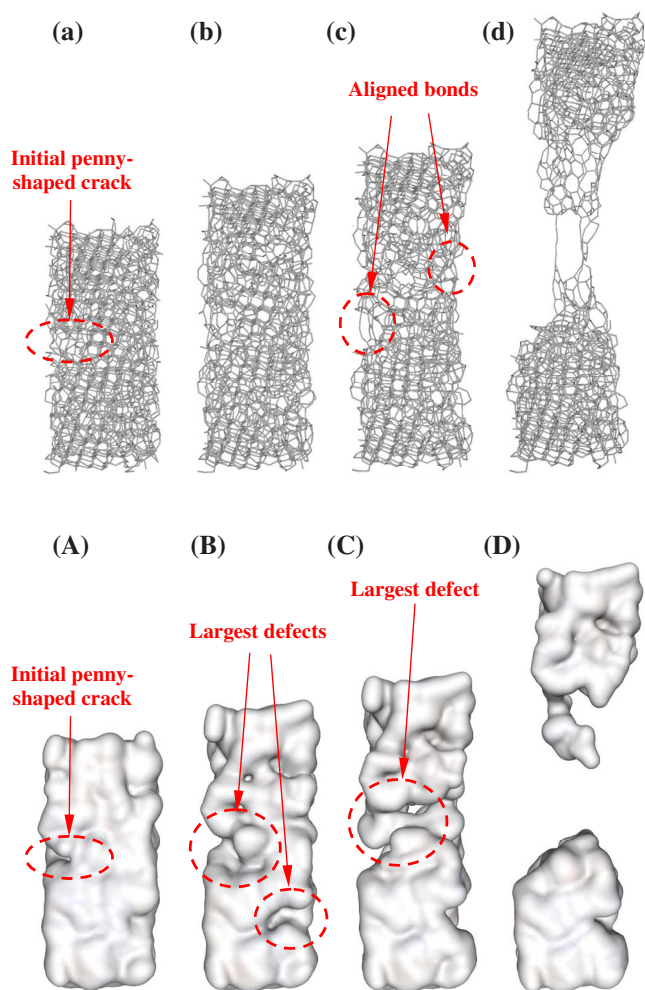


FIG. 6. (Color online) [(a)–(d)] Stick models and [(A)–(D)] surfaces of fourfold coordinated atom in amorphous carbon (2016 atoms) with an initial crack of diameter of 6 Å during the fracture process: [(a) and (A)] at 0 strain, [(b) and (B)] at stress, 12% strain, [(c) and (C)] at 27% strain, and [(d) and (D)] final structure at 79% strain.

defects lead to the failure of the amorphous carbon body. Nucleation and coalescence of voidlike defects do not occur in diamond; this absence of voids is typical of crystalline fracture.

(v) The fracture properties of diamond are more sensitive to small initial cracks than amorphous.

These characteristics of the fracture of amorphous carbon are likely due to its structural disorder, including (i) random bond directions, bond lengths, and bond angles, (ii) random hybridization levels, and (iii) initial small defects. Some of the initial defects are nearly the size of the initial crack, so the inserted crack apparently only affects the fracture process in its vicinity and does not have a substantial impact on the overall fracture process. We will substantiate this hypothesis in Sec. IV by studies of two-dimensional random networks.

The characteristics of fracture in amorphous carbon are quite similar to those in ductile materials, where voidlike defect growth and coalescence are important mechanisms.²⁵ In amorphous carbon nanospecimens, the voidlike defects are quite small, and other mechanisms such as rotation of

bonds play a role, but voidlike defect growth is definitely a key phenomenon in the decreased effect of initial defects.

The gradual nature of the failure process of amorphous carbon may be due to several factors. First, due to the structural heterogeneity of amorphous carbon, the energy or force required to successively break atomic bonds at the crack tip varies as the crack and the damage zone develop, since the angles of successive bonds change markedly. Secondly, part of the elastic energy is dissipated through local structural rearrangement, voidlike defect growth, and other irreversible structural changes.

Bond rearrangement plays an important role in the later stages. The carbon bonds, which are randomly oriented in the initial amorphous carbon structure, rotate to align with the loading direction at large strains, as shown in Fig. 2(c). At very large strains, fibrils composed of carbon-carbon single bonds are formed [Fig. 2(d)] and take some load even at tensile strain as large as 80%. We have commented on this in the previous section.

Interestingly, similar strengthening mechanisms are also seen in the tensile failure of glassy polymers. In glassy polymers, such as polystyrene and polymethyl methacrylate, failure is accompanied by “crazing.” During crazing, microvoids nucleate in front of the crack tip, and the polymer molecules between the voids are stretched in the loading direction and form chains and fibrils, which increases the resistance to fracture.²⁶ Due to the toughening effects of these molecular chains and fibrils, the material can sustain a substantial load at large strains and fails gradually. There are also similarities between our simulation results and failure simulations of glassy polymers.²⁷

C. Dependence of fracture strength on crack size

In this section, we compare the fracture strengths for amorphous carbon and diamond obtained by MD simulations with Griffith theory. The Griffith theory gives a lower bound on the fracture strength of a body by equating the surface energy needed for the crack to propagate with the elastic energy released by the body. It is a thermodynamic principle and gives a rigorous lower bound on the fracture stress. The only sources of error are the assumption of linear elastic response that is made in developing formulas for the energy released by the body and its neglect of lattice trapping.^{28,29} For a linear elastic, isotropic body of width h and a penny-shaped edge crack with radius c , the Griffith fracture stress is³⁰

$$\sigma_f = \left(\frac{\pi E \gamma}{2c(1-\nu^2)} \right)^{1/2} \frac{1-0.25c/h}{0.66} \quad \text{for } 0 < c/h \leq 0.4, \quad (1)$$

where γ is the surface energy, E is Young’s modulus, and ν is Poisson’s ratio.

To compute the Griffith fracture stress by Eq. (1), we obtained the surface energy γ by MD simulations by creating ten surfaces by pulling apart a specimen by prescribing the displacements of all atoms in the specimen. The surface energy is the net increase of the total energy. Descriptions for this method of calculating surface energy can be found in

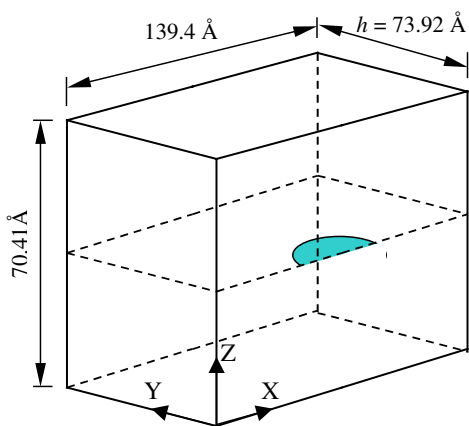


FIG. 7. (Color online) Geometries of the initial surface penny-shaped crack on a diamond/amorphous carbon cluster; x - z is a plane of symmetry.

literature.^{8,31} The surface energy γ for the amorphous carbon was found to be 2.80 J/m² with EDIP; the surface energy γ for diamond in the $\langle 111 \rangle$ surface was computed by the Brenner potential to be 5.40 J/m² by Shenderova *et al.*,³² and we used that value.

For the diamond fracture simulations, the Brenner second-generation REBO potential³² with a modification of its cut-off function was used (to improve its simulation of bond breaking⁹) for it has been checked more extensively in crystalline carbon materials.

Figure 8 compares the fracture strengths for diamond with the Griffith formula [Eq. (1)]. The calculated fracture strength is generally in good agreement with the Griffith equation for cracks with radii from 20 to 90 Å. The errors for small radii can be attributed to the fact that the cracks (created by removing atoms) are not perfectly penny shaped, since it is impossible to obtain a circular crack by removal of atoms at this scale. Furthermore, the Griffith equation does not account for the nonlinearity of the diamond near fracture nor lattice trapping. For cracks larger than 90 Å, the fracture strength deviates from the Griffith equation due to inapplicability of Eq. (2) when the free boundaries are too close to the crack. Similar good agreement with the Griffith equation for

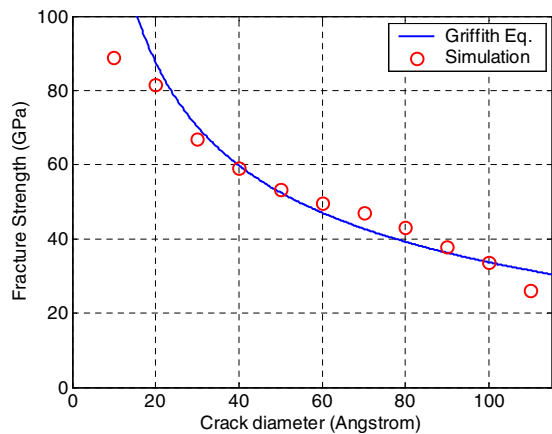


FIG. 8. (Color online) Dependence of fracture strength on crack size for diamond, compared with the Griffith formula.

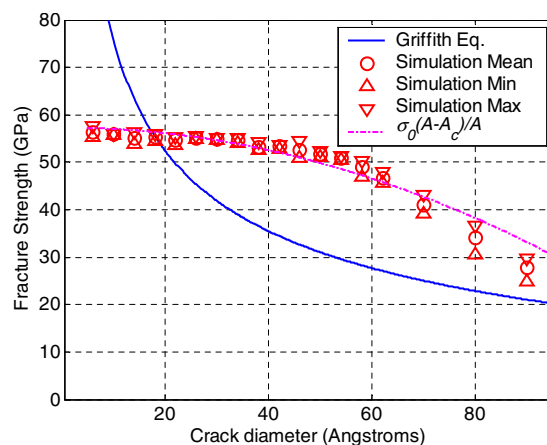


FIG. 9. (Color online) Dependence of fracture strength on the crack size for amorphous carbon nanospecimens ($149.0 \times 75.2 \times 79.0 \text{ \AA}^3$), showing the mean, minimum, and maximum strengths of three sample sets, and compared with the Griffith equation.

nanoscale cracks were found for SiC (Ref. 31) and grapheme sheets.⁸

For the simulations of amorphous carbon with defects, three pristine amorphous carbon samples were generated with simulated annealing. For each sample, a penny-shaped edge crack was created by removing a plane of carbon atoms; the geometry is similar to the diamond sample shown in Fig. 7, except that the amorphous carbon clusters were slightly smaller ($122.9 \times 61.28 \times 63.20 \text{ \AA}^3$).

The mean, minimum, and maximum of the three fracture strengths obtained from the simulations are compared with the Griffith formula, i.e., Eq. (1), in Fig. 9. Rather than exhibiting an inverse square root dependence on the crack radius c , i.e., a $c^{-1/2}$ dependence, as predicted by the Griffith equation, the fracture strength of amorphous carbon is almost constant for crack diameters smaller than about 40 Å. In Fig. 9 we also plot a σ_F curve, where

$$\sigma_F = \sigma_0 \frac{A - A_c}{A}, \quad (2)$$

where σ_0 is the fracture strength for the pristine amorphous carbon, A is the cross-sectional area, and A_c is the area of the crack. The fracture strengths from the simulations agree with the σ_F fairly well up to 70 Å. This implies that the fracture strength is governed by the cross-sectional area ($A - A_c$) that remains after the insertion of the initial crack. Thus, the strength of these nanospecimens of amorphous carbon is governed primarily by the cross-sectional area normal to the loading, rather than the brittle fracture behavior that governs diamond, which is reflected in the Griffith formula.

Even for the largest flaws studied here (85 Å), the computed strength of 25 GPa is markedly greater than the experimental results of Robertson,¹ 6–9 GPa; the fracture strains reported in those experiments are of the order of 1.2%, which is one-tenth of our computed values. This suggests that the experimental specimens contained much larger flaws and that flaw insensitivity may not persist for larger scales. Un-

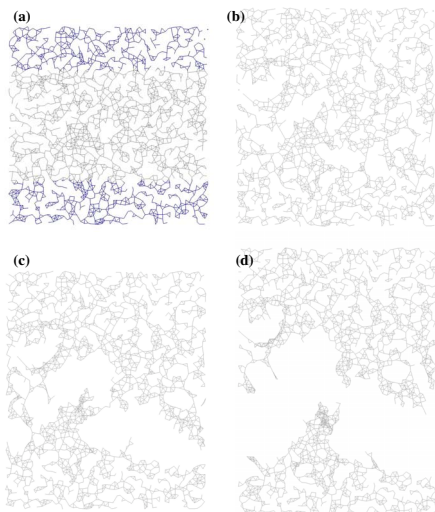


FIG. 10. (Color online) Evolutions for a random network with $\bar{m}=3.7$ (a) at 0 strain (boundary atoms in dark blue) (b) at maximum stress (10.7 strain), (c) at 20% strain, and (d) at maximum (50%) strain.

fortunately, such large flaws are beyond our computational capabilities at this time.

IV. RANDOM NETWORK MODEL

To explore to what extent the properties of amorphous carbon can be attributed to the randomness of its atomic structure, we considered two-dimensional random networks with a simpler potential. The substantially lower computational cost of these random network models made it possible to study larger specimens.

In our two-dimensional random network models, the positions of the atoms were generated from a Matern two-dimensional random field.³³ The Matern random field is a thinned Poisson random field. The network generation consists of two steps: (i) the random coordinates of a group of atoms based on a uniform distribution on a rectangular plane are independently generated; (ii) the neighboring atoms of each atom are checked, and neighboring atoms are deleted if they are closer than a specified distance h . Then, atoms are connected with bonds if they are within a cut-off distance $r_c=1.80$. All units are nondimensional.

A key property of a random network models is its connectivity, defined by

$$\bar{m} = \frac{1}{N} \sum_{i=1}^N m_i, \quad (3)$$

where N is the total number of atoms and m_i is the number of neighbors connected to atom i . By adjusting the deletion distance h , the density and the connectivity of the network can be easily modified.

Figure 10(a) shows a random network generated with this method for a 64.73×64.73 specimen with 1854 atoms. In the following simulations, \bar{m} is chosen to be 3.7, which is a typical average coordination number in tetrahedral amorphous carbon.

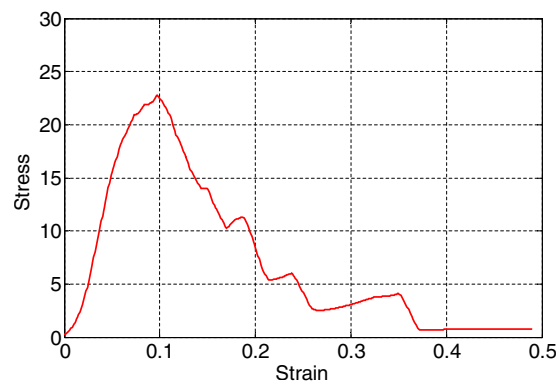


FIG. 11. (Color online) Stress-strain curve for 2D random network fracture with 1854 atoms.

A MD scheme is used for the simulations. The interaction between atoms is described by a bond-stretching potential of the Morse type:

$$E_p = \sum_{j>i} \phi_{ij}(r_{ij} - r_{ij}^0), \quad (4)$$

$$\phi_{ij}(r_{ij} - r_{ij}^0) = \begin{cases} D_e(1 - e^{-\alpha(r_{ij} - r_{ij}^0)})^2 & \text{if } r_{ij} \leq \alpha_f r_{ij}^0 \\ 0 & \text{if } r_{ij} > \alpha_f r_{ij}^0, \end{cases} \quad (5)$$

where E_p is the potential energy, ϕ_{ij} is the energy contributed by the bond connecting atoms i and j , r_{ij} and r_{ij}^0 are the instantaneous and initial distances between atoms i and j , respectively, D_e is 188.2, and α is 2.625. For each bond, its equilibrium length is its initial length so that the network is initially in equilibrium. A bond is considered broken if it is longer than $1.20r_{ij}^0$.

The results from a typical simulation of the random network with 1854 atoms are shown in Fig. 11. The stress-strain curve is qualitatively similar to the fracture of amorphous carbon shown in Fig. 1.

Figures 10(a)–10(d) show line models of the specimen: (a) at 0 strain (with boundary atoms in dark blue), (b) at the maximum stress (10.7% strain), (c) at 20% strain, and (d) at the maximum (50%) strain. Cracks and voids are apparent in the initial unstrained specimen [Fig. 10(a)]. At the maximum stress, these small defects coalesce to form larger voids [Fig. 10(b)]. These voids continue to grow and coalesce, and only a few loading paths remain at about strain of 20%, Fig. 10(c). The specimen fails at 38%, Fig. 10(d). A recent study of two-dimensional (2D) random network fracture³⁴ reported similar stages of fracture.

As in amorphous carbon, for the random network, the following are observed:

(i) The fracture is gradual rather than catastrophic, the stress-strain curves have similar increasing, softening, and plateauing stages, and the maximum strain is larger compared to the fracture strain.

(ii) Fracture is accompanied by the growth and coalescence of multiple initial defects, rather than the growth of a single dominant crack.

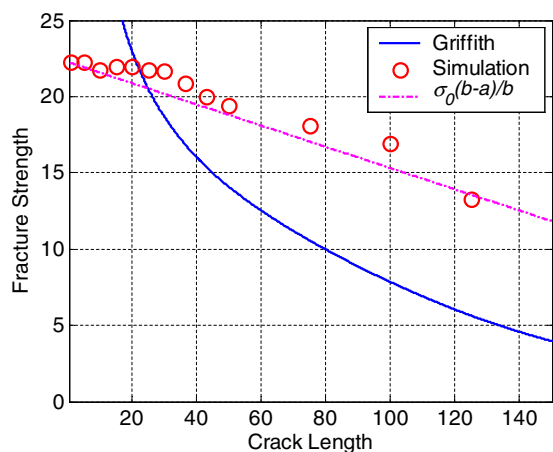


FIG. 12. (Color online) Fracture strength vs crack size for a 2D random network with 49 114 atoms and dimensions of 320×320 .

The fracture strengths for a plate of width $2b$ with a center crack of lengths $2a$ under uniform tension obtained by the Griffith formula³⁵

$$\sigma_f = \sqrt{\frac{2E\gamma}{\pi a} \frac{1}{1.0 + 0.128\left(\frac{a}{b}\right) - 0.288\left(\frac{a}{b}\right)^2 + 1.523\left(\frac{a}{b}\right)^3}} \quad (6)$$

for $0 < a/b < 0.7$

are compared to the simulation results in Fig. 12. The simulation results for the fracture strength are almost independent of crack size for cracks shorter than 30. The strength decreases significantly for cracks longer than 35, which is partly due to the finite size of our specimen (320×320). The insensitivity of fracture strength to small cracks shown in Fig. 12 is similar to that found in the amorphous carbon (Fig. 9).

In Fig. 12, we also show σ_F given by

$$\sigma_F = \sigma_0 \frac{b-a}{b}. \quad (7)$$

This indicates that in the random network, just as in the amorphous carbon, the strength depends on the loaded area. This contrasts with brittle fracture behavior, in which the strength varies with $a^{-1/2}$, as shown in Eq. (6).

V. SUMMARY

We have used MD simulations and the EDIP to study the fracture of tetrahedral amorphous carbon nanospecimens. We found that EDIP is advantageous in simulations of amorphous carbon as compared to the Brenner or Tersoff poten-

tials because it yields sp^3 fractions, elastic moduli, and fracture stresses and strains that are in better agreement with experiment and higher order calculations. We have found that tetrahedral amorphous carbon nanospecimens fracture very differently from diamond nanospecimens: (i) failure is gradual instead of catastrophic, (ii) it is accompanied with voidlike defect growth and coalescence, and (iii) the fracture strength is insensitive to initial cracks below about 40 Å. These fracture characteristics appear to result from the structural disorder of amorphous carbon.

The insensitivity of the fracture strength of amorphous carbon nanospecimens to cracklike flaws below a critical size is of particular interest. The strengths of specimens with cracks below a critical size are almost identical to that of pristine specimens. This indicates a flaw tolerance such as that proposed by Gao *et al.*² Our results show that such flow tolerance does not occur in the crystalline form of carbon, i.e., diamond. Flaw tolerance in crystalline structures has also been disputed by Ballarini *et al.*³⁶

An examination of the failure process in amorphous carbon and diamond revealed several factors that may explain this flaw tolerance in amorphous carbon nanospecimens and its absence in diamond nanospecimens. Failure in amorphous carbon involves the growth of voidlike defects and significant rotation of bonds into alignment with the loading direction. The growth of voidlike defects depends very little on preexisting flaws, since amorphous carbon already possesses many anomalies because of its disordered structure. By contrast, in diamond, fracture does not involve voidlike defect growth but instead consists of the rapid sequential breakage of bonds adjacent to the flaw. Thus, any preexisting flaw has significant effects on the strength of diamond.

To assess the degree to which the observed behavior in amorphous carbon is due to its random structure, we also studied two-dimensional random networks. We found that the fracture of random networks is similar to that observed in amorphous carbon: gradual failure, accompanied by void growth and coalescence and insensitivity of fracture strength to initial cracks below a critical dimension. These shared attributes of amorphous carbon and random network fracture support our hypothesis that structural disorder is the major causative factor of the differences between fracture in amorphous carbon and diamond.

ACKNOWLEDGMENTS

The authors gratefully acknowledge the grant support from the NASA University Research, Engineering and Technology Institute on Bio Inspired Materials (BIMat) under Award No. NCC-1-02037, the support of the Department of Energy, Sandia National Laboratory, and the Army Research Office under Grant No. W911NF-05-1-0049.

*tedbelytschko@northwestern.edu

- ¹J. Robertson, *Mater. Sci. Eng., R.* **37**, 129 (2002).
- ²H. J. Gao, B. H. Ji, I. L. Jager, E. Arzt, and P. Fratzl, *Proc. Natl. Acad. Sci. U.S.A.* **100**, 5597 (2003).
- ³M. G. Fyta, I. N. Remediakis, P. C. Kelires, and D. A. Papaconstantopoulos, *Phys. Rev. Lett.* **96**, 185503 (2006).
- ⁴J. T. Paci, T. Belytschko, and G. C. Schatz, *Phys. Rev. B* **74**, 184112 (2006).
- ⁵M. F. Yu, O. Lourie, M. J. Dyer, K. Moloni, T. F. Kelly, and R. S. Ruoff, *Science* **287**, 637 (2000).
- ⁶Q. Lu, Ph.D. thesis, University of Delaware, 2005.
- ⁷T. Belytschko, S. P. Xiao, G. C. Schatz, and R. S. Ruoff, *Phys. Rev. B* **65**, 235430 (2002).
- ⁸R. Khare, S. L. Mielke, J. T. Paci, S. Zhang, G. C. Schatz, and T. Belytschko, *Phys. Rev. B* **75**, 075412 (2007).
- ⁹S. L. Mielke, D. Troya, S. Zhang, J. L. Li, S. P. Xiao, R. Car, R. S. Ruoff, G. C. Schatz, and T. Belytschko, *Chem. Phys. Lett.* **390**, 413 (2004).
- ¹⁰T. Dumitrica, T. Belytschko, and B. I. Yakobson, *J. Chem. Phys.* **118**, 9485 (2003).
- ¹¹H. D. Espinosa, B. Peng, B. C. Prorok, N. Moldovan, O. Auciello, J. A. Carlisle, D. M. Gruen, and D. C. Mancini, *J. Appl. Phys.* **94**, 6076 (2003).
- ¹²J. T. Paci, T. Belytschko, and G. C. Schatz, *Chem. Phys. Lett.* **414**, 351 (2005).
- ¹³J. E. Field and C. S. J. Pickles, *Diamond Relat. Mater.* **5**, 625 (1996).
- ¹⁴Q. K. Li and M. Li, *Appl. Phys. Lett.* **87**, 269901 (2005).
- ¹⁵N. A. Marks, *Phys. Rev. B* **63**, 035401 (2001).
- ¹⁶J. Tersoff, *Phys. Rev. Lett.* **61**, 2879 (1988).
- ¹⁷D. W. Brenner, O. A. Shenderova, J. A. Harrison, S. J. Stuart, B. Ni, and S. B. Sinnott, *J. Phys.: Condens. Matter* **14**, 783 (2002).
- ¹⁸O. A. Shenderova, D. W. Brenner, and L. H. Yang, *Phys. Rev. B* **60**, 7043 (1999).
- ¹⁹H. U. Jager and K. Albe, *J. Appl. Phys.* **88**, 1129 (2000).
- ²⁰N. Marks, *J. Phys.: Condens. Matter* **14**, 2901 (2002).
- ²¹N. A. Marks, N. C. Cooper, D. R. McKenzie, D. G. McCulloch, P. Bath, and S. P. Russo, *Phys. Rev. B* **65**, 075411 (2002).
- ²²N. A. Marks, M. F. Cover, and C. Kocer, *Appl. Phys. Lett.* **89**, 131924 (2006).
- ²³H. E. Troiani, M. Miki-Yoshida, G. A. Camacho-Bragado, M. A. L. Marques, A. Rubio, J. A. Ascencio, and M. Jose-Yacamán, *Nano Lett.* **3**, 751 (2003).
- ²⁴K. Asaka and T. Kizuka, *Phys. Rev. B* **72**, 115431 (2005).
- ²⁵T. L. Anderson, *Fracture Mechanics: Fundamentals and Applications* (CRC, Boca Raton, FL, 1995).
- ²⁶R. Estevez and E. Van der Giessen, in *Intrinsic Molecular Mobility and Toughness of Polymers II*, edited by H. H. Kausch (Springer, Berlin, 2005), Vol. 188, p. 195.
- ²⁷U. Kulmi and S. Basu, *Modell. Simul. Mater. Sci. Eng.* **14**, 1071 (2006).
- ²⁸J. R. Rice, *J. Mech. Phys. Solids* **26**, 61 (1978).
- ²⁹R. Thomson, C. Hsieh, and V. Rana, *J. Appl. Phys.* **42**, 3154 (1971).
- ³⁰G. P. Cherepanov, *Mechanics of Brittle Fracture* (McGraw-Hill, New York, 1979).
- ³¹A. Mattoni, L. Colombo, and F. Cleri, *Phys. Rev. Lett.* **95**, 115501 (2005).
- ³²O. A. Shenderova, D. W. Brenner, A. Omeltchenko, X. Su, and L. H. Yang, *Phys. Rev. B* **61**, 3877 (2000).
- ³³B. Matern, *Spatial Variation* (Springer-Verlag, Berlin, 1986).
- ³⁴I. Malakhovskiy and M. A. J. Michels, *Phys. Rev. B* **74**, 014206 (2006).
- ³⁵E. E. Gdoutos, *Fracture Mechanics: An Introduction* (Springer, Dordrecht, 2005).
- ³⁶R. Ballarini, R. Kayacan, F. J. Ulm, T. Belytschko, and A. H. Heuer, *Int. J. Fract.* **135**, 187 (2005).